

VU Research Portal

Development of PET tracers for in vivo imaging of active tissue transglutaminase

van der Wildt, B.

2017

document version

Publisher's PDF, also known as Version of record

[Link to publication in VU Research Portal](#)

citation for published version (APA)

van der Wildt, B. (2017). *Development of PET tracers for in vivo imaging of active tissue transglutaminase*.

General rights

Copyright and moral rights for the publications made accessible in the public portal are retained by the authors and/or other copyright owners and it is a condition of accessing publications that users recognise and abide by the legal requirements associated with these rights.

- Users may download and print one copy of any publication from the public portal for the purpose of private study or research.
- You may not further distribute the material or use it for any profit-making activity or commercial gain
- You may freely distribute the URL identifying the publication in the public portal ?

Take down policy

If you believe that this document breaches copyright please contact us providing details, and we will remove access to the work immediately and investigate your claim.

E-mail address:

vuresearchportal.ub@vu.nl

Chapter 5

***In vivo* evaluation of two TG2 PET tracers in an orthotopic MDA-MB-231 tumour xenograft model**

Berend van der Wildt, Micha M.M. Wilhelmus, Wissam Beaino, Esther J.M. Kooijman, Robert C. Schuit, John G.J.M. Bol, John J.P. Breve, Ralf Pasternack, Adriaan A. Lammertsma, Albert D. Windhorst, Benjamin Drukarch.

Submitted

Abstract

The protein cross-linking enzyme tissue transglutaminase (TG2; EC 2.3.2.13) is associated with the pathogenesis of various diseases, including cancer. Recently, the synthesis and initial evaluation of two high-potential radiolabelled irreversible TG2 inhibitors was reported by us. In the present study, these two compounds were evaluated further in a breast cancer (MDA-MB-231) tumour xenograft model for imaging active tissue transglutaminase *in vivo*. The metabolic stability of [¹¹C]**3** and [¹⁸F]**6g** in SCID mice was comparable to the previously reported stability in Wistar rats. Quantitative real-time polymerase chain reaction analysis on MDA-MB-231 cells and isolated tumours showed a high level of TG2 expression with very low expression of other transglutaminases. PET imaging showed low tumour uptake of [¹¹C]**3** (approx. 0.2 percentage of the injected dose per gram (%ID/g) at 40-60 min p.i.) and with relatively fast washout. Tumour uptake for [¹⁸F]**6g** was steadily increasing over time (approx. 1.7 %ID/g at 40-60 min p.i.). Pretreatment of the animals with the TG2 inhibitor **ERW1041E** resulted in lower tumour activity concentrations and this inhibitory effect was enhanced using unlabelled **6g**. Whereas the TG2 targeting potential of [¹¹C]**3** in this model seems inadequate, targeting of TG2 using [¹⁸F]**6g** was achieved.

5.1 Introduction

Transglutaminases comprise a family of enzymes responsible for the calcium-dependent intra- and intermolecular crosslinking of proteins between the side chains of glutamine and lysine residues, forming an epsilon-(gamma-glutamyl)-lysine bond [1]. Tissue transglutaminase (TG2) is ubiquitously expressed and, under physiological conditions, plays a role in *e.g.* apoptosis, cell differentiation and cell migration [2, 3]. The crosslinking activity of this enzyme is tightly regulated by various mechanisms. First, TG2 exists in two distinct conformations, referred to as closed and open conformations, respectively [4, 5]. Only in the open conformation, which is associated with high calcium and low guanosine diphosphate/guanosine triphosphate (GDP/GTP) concentrations, the active site cysteine residue is exposed and transamidation can be expected [5]. In the closed conformation, two consecutive C-terminal β -barrels sterically limit transamidation activity [4]. Second, the redox state of TG2 determines its catalytic activity, since a Cys370-Cys371 disulphide bridge, despite locking TG2 in its open conformation, hampers transamidation [6]. Finally, crosslinking activity of TG2 is regulated by formation of ternary protein complexes on the cell surface with extracellular matrix proteins, such as fibronectin and membrane-bound integrins [7]. Clearly, this multitude of regulatory mechanisms poses a challenge for assessing TG2 crosslinking activity *in vivo*. Often changes in TG2 expression levels or immunohistochemical detection of epsilon-(gamma-glutamyl)-lysine bonds are used as *ex vivo* biomarkers of TG2 activity. Alternatively, transglutaminase mediated incorporation of systemically administered biotin-labelled amine substrates can be detected immunohistochemically after sacrificing the test animal [8, 9].

TG2 is strongly associated with the pathogenesis of cancer, celiac disease, and fibrotic and neurodegenerative diseases [10-15], in which its role is assumed to be related to its cross-linking activity. The fact that TG2 knock-out mice are

phenotypically healthy in a stress free environment has further boosted TG2 as a potential target for therapeutic intervention [16]. Nowadays, a wide array of TG2 inhibitors has been developed [17]. Nevertheless, further development of potent inhibitors towards clinical studies, for example by evaluation in animal models, has been limited. The availability of a validated TG2 PET tracer is likely to stimulate *in vivo* research of potent TG2 inhibitors [18].

Recently, carbon-11 and fluorine-18 labelled small molecule TG2 PET tracers have been developed by our group [19, 20]. [^{11}C]**3** (figure 1) was selected out of three carbon-11 labelled TG2 inhibitors based on its superior metabolic stability. In addition, [^{18}F]**6g**, a peptidic TG2 inhibitor (figure 1), was developed. Despite being completely metabolised *in vivo* after just 15 min post injection, imaging with [^{18}F]**6g** was suggested as also the only radiometabolite was shown to be an equipotent inhibitor of TG2 [20]. Both selected compounds, [^{11}C]**3** and [^{18}F]**6g**, were able to discriminate between active and inactive tissue transglutaminase *in vitro* and demonstrated specific and selective binding to MDA-MB-231 tumour sections, as assessed by *in vitro* autoradiography experiments. However, *in vitro* autoradiography assays do not necessarily reflect *in vivo* biology. Therefore, the aim of the present study was to determine whether these new tracers are able to target TG2 also *in vivo*. To this end, compounds [^{11}C]**3** and [^{18}F]**6g** were evaluated in a mouse MDA-MB-231 tumour xenograft model.

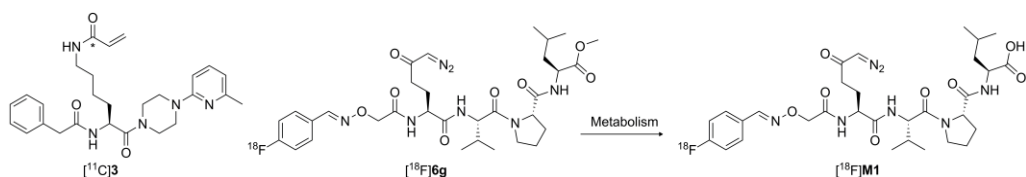


Figure 1: Chemical structures of the TG2 inhibitors [^{11}C]**3**, [^{18}F]**6g**, together with that of its *in vivo* formed metabolite [^{18}F]**M1** [19, 20]. The position of the carbon-11 label in [^{11}C]**3** is depicted by *.

5.2 Materials and Methods

5.2.1 Cell culture

MDA-MB-231 human breast cancer cells were purchased from American Type Culture Collection (Rockville, MD, USA). Cells were cultured at 37 °C, 5% CO₂ in Dulbecco's Modified Eagle Medium with 4.5 g/L glucose (Lonza, Basel, Switzerland) with HEPES supplemented with L-glutamine and fetal calf serum (5%).

5.2.2 Xenograft model

Severe combined immunodeficient (SCID) female mice (6-8 weeks, 20 to 25 g, Charles River, Wilmington, MA, USA) were housed in sterile cages under standard conditions (24 °C, 60% relative humidity, 12 h light/dark cycles) and provided with water and food *ad libitum*. MDA-MB-231 cells (1×10^6) were injected orthotopically in the fat pad of the second thoracic mammary glands (bilateral) [21]. Tumour dimensions were measured using a Vernier calliper and tumour volume was calculated using the formula $(x^2 \cdot y)/2$ (x and y being the width and length, respectively) for an ellipsoid. At 8 weeks after MDA-MB-231 cell injection, tumours reached the target size (200 mm³, figure 2).

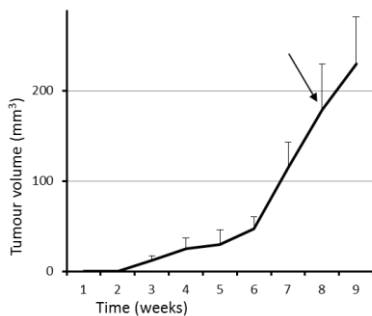


Figure 2: Tumour growth curves (number of animals = 8, number of tumours = 16). Error bars indicate standard deviations; the arrow indicates start of the PET scanning experiments.

This study was performed according to national regulations and was approved by the Animal Experimentation Ethics Committee of the VU University Medical Center.

5.2.3 QPCR analysis

Total messenger ribonucleic acid (mRNA) was isolated from MDA-MB-231 tumour cells or tumour tissue using Trizol Reagent (Invitrogen, Carlsbad, CA, USA) according to the manufacturer's instructions. RNA was reverse-transcribed into complementary deoxyribonucleic acid (cDNA) using the High-Capacity cDNA Reverse Transcription kit (Applied Biosystems, Foster City, Ca, USA) using 0.5 µg oligo-dT primers according to the manufacturer's instructions. For the subsequent quantitative real-time polymerase chain reaction (qPCR), the Power SYBR Green Master Mix (Applied Biosystems) was used. Primers were purchased from Eurogentec (Maastricht, Netherlands) and qPCR was performed in MicroAmp Optical 96-well Reaction Plates (Applied Biosystems) on a StepOnePlus Real-Time PCR system (Applied Biosystems). The reaction mixture (20 µL) was composed of 1 × Power SYBR Green buffer (Applied Biosystems), 3.75 pmol of each primer (see Table 1 for primer details), and 12.5 ng cDNA. The thermal cycling conditions were an initial 10 min at 95 °C followed by 50 cycles of 15 s at 95 °C and 1 min at 60 °C. The specificity of the reaction was checked by means of melt curve analysis. Relative expression levels of the target genes were determined by LinRegPCR software (version 2014.3; website: <http://www.hfrc.nl>) using the following equation $N_0 = N_q / (E^{C_q})$ (N_0 = target quantity, N_q = fluorescence threshold value, E = mean PCR efficiency per amplicon, C_q = threshold cycle) [22], after which the value was normalized to the expression level of the reference gene glyceraldehyde-3-phosphate-dehydrogenase (GAPDH) using the following formula ($N_{0, \text{gene of interest}} / N_{0, \text{GAPDH}}$). Results are expressed as gene expression relative to GAPDH ± standard deviation ($n = 4$ for both tumour cells and tumour tissue measurements).

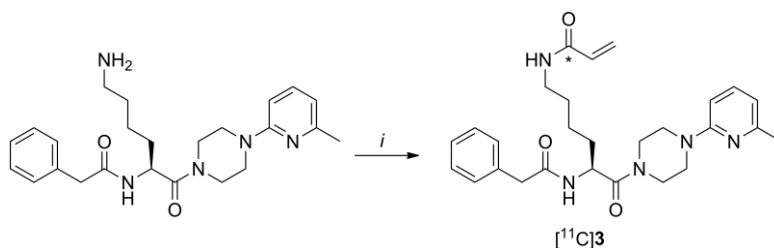
Table 1: Primer sequences used for qPCR analysis

Gene	NCBI Reference Sequence	Forward (5'→3')	Reverse (5'→3')	Amplicon Size (basepairs)
GAPDH	NM_002046.3	TCAAGGGCATCTGGGCTAC	CGTCAAAGGTGGAGGAGTGG	81
TGM1	NM_000359.2	CAATGTCTCAGGCCACGTC	CCAGTAACGTGAGGGAGAGG	95
TGM2	NM_004613.2	AGAGGAGCGGCAGGAGTATG	AGGATCCCATCTTCAAAGTGC	111
TGM3	NM_003245.3	AACCTGAAGATCGACGTGC	CAGTTGCTTGGTGCCACTC	93
TGM5	NM_201631.3	TCCTGGTGAACAAGATCATC	GTATGGAGAGTGGCTGGTTC	90
F13A1	NM_000129.3	TCCGACAGGGCAGTCTTTC	CCTGTGGGTAGCGACCAATGA	105

5.2.4 Radiotracer synthesis

5.2.4.1. *(S)*-N-(6-(4-(6-methylpyridin-2-yl)piperazin-1-yl)-6-oxo-5-(2-phenylacetamido)hexyl)[¹¹C]acrylamide (**[¹¹C]3**).

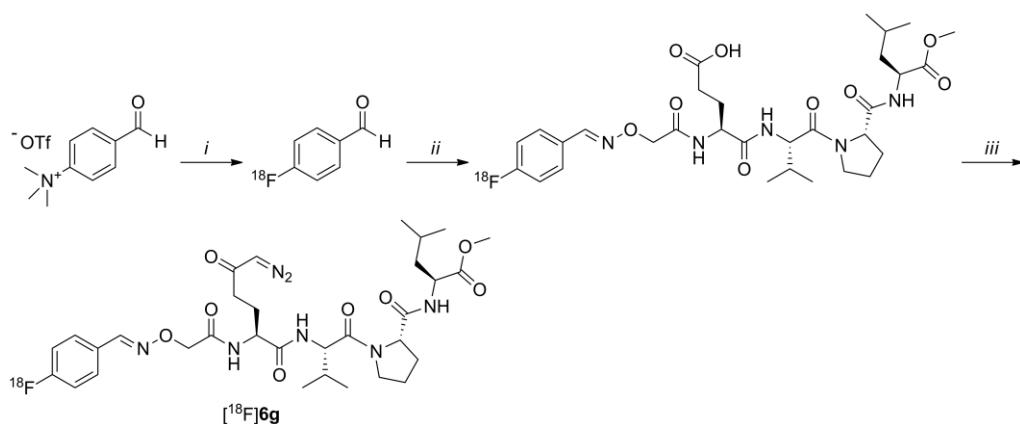
[¹¹C]3 was synthesized as previously described (scheme 1) [19] and was obtained in 20-28% decay corrected (d.c) yield based on [¹¹C]CO with a specific activity of 144 ± 22 GBq·μmol⁻¹ and a radiochemical purity >99% (n = 4). The identity of the product was confirmed by analytical high performance liquid chromatography (HPLC) analysis by co-injection of radiolabelled and unlabelled **3** using a Phenomenex Luna Phenyl-hexyl column (5 μm, 250 mm x 4.6 mm) with H₂O/Acetonitrile (MeCN), 7:3 (v/v) as eluent, retention time (R_t): 9.0 min.



Scheme 1: Radiosynthesis of **[¹¹C]3**. Reagents and conditions: i) [¹¹C]CO, vinyl iodide, Pd₂(dba)₃, PPh₃, tetrahydrofuran (THF), 5 min, 100 °C.

5.2.4.2. (*S*)-methyl 2-((*S*)-1-((7*S*,10*S*,*E*)-7-(4-diazo-3-oxobutyl)-1-(4-[¹⁸F]fluorophenyl)-10-isopropyl-5,8-dioxo-3-oxa-2,6,9-triazaundec-1-en-11-oyl)pyrrolidine-2-carboxamido)-4-methylpentanoate ([¹⁸F]**6g**).

[¹⁸F]**6g** was synthesized as previously described (scheme 2) [20] and was obtained in 3-4% d.c. yield, calculated at the time of the start of the synthesis, with a specific activity of 111 ± 28 GBq· μmol^{-1} and a radiochemical purity >98% ($n = 4$). The identity of the product was confirmed by analytical HPLC analysis by co-injection of radiolabelled and unlabelled **6g** using a Phenomenex Luna Phenyl-hexyl column (5 μm , 250 mm x 4.6 mm) with H₂O/MeCN/TFA, 60:40:0.1 (v/v/v) as eluent, R_t : 28 min.



Scheme 2: Radiosynthesis of [¹⁸F]**6g**. Reagents and conditions: *i*) K₂CO₃, [¹⁸F/K₂₂₂], DMF, 15 min, 100 °C; *ii*) (*S*)-4-(2-(aminooxy)acetamido)-5-(((*S*)-1-((*S*)-2-(((*S*)-1-methoxy-4-methyl-1-oxopentane-2-yl)carbamoyl)pyrrolidine-1-yl)-3-methyl-1-oxobutan-2-yl)amino)-5-oxopentanoic acid, trifluoroacetic acid (TFA), *N,N*-dimethylformamide (DMF)/THF, 30 min, 50 °C; *iii*) isobutylchloride, *N*-methylmorpholine, DMF/THF, 5 min, -10 °C, then CH₂N₂ (0.5 M in Et₂O), 30 min, -10 °C to rt.

5.2.5 Metabolite analysis

Healthy female SCID mice (20-25 g, Harlan, Horst, The Netherlands) were injected in the tail vein with [^{11}C]**3** or [^{18}F]**6g** (20 MBq) under isoflurane anaesthesia (2% in O_2 at $1 \text{ L} \cdot \text{min}^{-1}$). Mice were sacrificed at 15 and 45 min post injection ($n = 3$ for each time-point) by cervical dislocation. Blood ($\sim 0.5 - 1 \text{ mL}$) was withdrawn by heart puncture, collected in a heparin coated tube and centrifuged at 5000 RPM to separate plasma from blood cells. Solid phase extraction (SPE) cartridges (tC18, Waters, Milford, MA, USA) were preconditioned by washing with methanol (MeOH, 6 mL) and H_2O (2 times 6 mL). Plasma ($\sim 0.2 \text{ mL}$) was mixed with 0.15 M HCl (0.2 mL) and loaded on the tC18 cartridge. The polar fraction was obtained by elution of the cartridge with H_2O (3 mL), the non-polar fraction by subsequent elution with MeOH (1.5 mL) and H_2O (0.5 mL). Both fractions were counted for radioactivity in a gamma counter. The percentage of intact tracer in the non-polar fraction was determined by online and offline HPLC analysis (Gemini C18 column ($5 \mu\text{m}$, $10 \text{ mm} \times 250 \text{ mm}$, Phenomenex, Torrance, CA, USA) with eluent MeCN (A) and 0.1% TFA acid in H_2O (B) as eluent according to the following schemes; For [^{11}C]**3**: 0min, 70% B at $0.25 \text{ mL} \cdot \text{min}^{-1}$; 0.5 min, 70% B at $3.5 \text{ mL} \cdot \text{min}^{-1}$; 9.0 min, 10% B at $3.5 \text{ mL} \cdot \text{min}^{-1}$; 12.0 min, 10% B at $3.5 \text{ mL} \cdot \text{min}^{-1}$; 12.5 min, 70% B at $3.5 \text{ mL} \cdot \text{min}^{-1}$; 14.5 min, 70% B at $3.5 \text{ mL} \cdot \text{min}^{-1}$ and 15 min, 70% B at $0.25 \text{ mL} \cdot \text{min}^{-1}$ or for [^{18}F]**6g**: 0 min, 80% B at $0.25 \text{ mL} \cdot \text{min}^{-1}$; 0.5 min, 80% B at $3 \text{ mL} \cdot \text{min}^{-1}$; 6.0 min, 30% B at $3 \text{ mL} \cdot \text{min}^{-1}$; 12.0 min, 30% B at $3 \text{ mL} \cdot \text{min}^{-1}$; 12.5 min, 80% B at $3.0 \text{ mL} \cdot \text{min}^{-1}$; 14.5 min, 80% B at $3.0 \text{ mL} \cdot \text{min}^{-1}$; 15.0 min, 80% B at $0.25 \text{ mL} \cdot \text{min}^{-1}$ ($R_t = 11.5 \text{ min}$). Offline HPLC analysis was performed when the online HPLC analysis yielded a low signal to noise ration. For offline analysis, HPLC fractions (30 s per fraction) were collected and counted for radioactivity (WIZARD 2480 Compugamma, PerkinElmer, Waltham, MA, USA). The counting results were plotted to generate the corresponding HPLC chromatograms. Data were expressed as percentage of intact tracer, polar metabolites and non-polar metabolites \pm standard deviation.

5.2.6 Metabolite characterization

To healthy SCID mice ($n = 2$) 10 MBq [^{18}F]**6g** diluted with 50 μg ($2.5 \text{ mg}\cdot\text{kg}^{-1}$) of unlabelled **6g** was administered, corresponding to a specific activity of $0.14 \text{ GBq}\cdot\mu\text{mol}^{-1}$. At 30 min post injection, animals were sacrificed under isoflurane anaesthesia (2% in O_2 at $1 \text{ L}\cdot\text{min}^{-1}$) by cervical dislocation. Blood ($\sim 1 \text{ mL}$) was collected by heart puncture. Blood plasma was separated using a SPE procedure as described in 'Metabolite analysis' (*vide supra*). The non-polar fraction was analysed by HPLC and Liquid chromatography – tandem mass spectrometry (LC-MS/MS) in multiple reaction monitoring (MRM) mode. LC-MS/MS analysis was performed on a Jasco system (Easton, PA, USA) with an AB Sciex QTRAP 5500 mass spectrometer (Concorde, Ontario, Canada). The Jasco system consisted of two pumps (X-LC 3180PU), a degasser (X-LC 3080DG), a mixer (X-LC 3080MX), a column oven (X-LC 3080CO) and databoxes LV 2080-03 and LC-Net II/ACD. A Kinetex C18 column ($1.7 \mu\text{m}$, 100 Å, $100 \times 2.10 \text{ mm}$, Phenomenex, Torrance, CA, USA) at $25 \text{ }^\circ\text{C}$ was used for chromatographic separation with eluent MeCN (A) and 0.1% formic acid in H_2O (B) according to the following scheme: 0 min, 90% B at $0.5 \text{ mL}\cdot\text{min}^{-1}$; 3 min, 10% B at $0.5 \text{ mL}\cdot\text{min}^{-1}$; 5 min, 10% B at $0.5 \text{ mL}\cdot\text{min}^{-1}$; 5.5 min 90% B at $0.5 \text{ mL}\cdot\text{min}^{-1}$. Capillary potential was set at 5.5 kV, source temperature at $100 \text{ }^\circ\text{C}$, and desolvation temperature at $750 \text{ }^\circ\text{C}$. MRM Q1 and Q3 set at: m/z 696.2-418.0 for detection of compound **6g** and m/z 682.1-626.3 for detection of **M1**.

5.2.7 Chemical synthesis

5.2.7.1 General

All reagents were obtained from commercial sources (Sigma Aldrich, St. Louis, USA). Solvents were obtained from Biosolve (Valkenswaard, the Netherlands) and used as received unless stated otherwise. Dichloromethane (DCM) and DMF were dried over activated 3 \AA molecular sieves. THF was first distilled from LiAlH_4 and then stored on

activated 3 Å molecular sieves. Reaction monitoring by thin layer chromatography was performed on pre-coated silica 60 F254 aluminium plates (Merck, Darmstadt, Germany). Spots were visualized by UV light or ninhydrin. Evaporation of solvents was performed under reduced pressure at 40 °C using a rotary evaporator. Flash column chromatography was performed manually on Silica gel 60 Å (Merck, Darmstadt, Germany). Nuclear magnetic resonance (NMR) spectroscopy was performed using a Bruker (Billerica, MA, USA) Avance 250 (250.13 MHz for ¹H and 62.90 MHz for ¹³C) or an Avance 500 (500.23 MHz for ¹H and 125.78 MHz for ¹³C) with chemical shifts (δ) reported in parts per million (ppm) relative to the solvent (chloroform (CDCl₃), ¹H: 7.26 ppm, ¹³C: 77.16 ppm). Electrospray ionisation-high resolution mass spectrometry (ESI-HRMS) was carried out using a Bruker microTOF-Q instrument in positive ion mode (capillary potential of 4500 V).

5.2.7.2. *(S)*-methyl 2-((*S*)-1-((7*S*,10*S*)-7-(4-diazo-3-oxobutyl)-1-(4-fluorophenyl)-10-isopropyl-5,8-dioxo-3-oxa-2,6,9-triazaundec-1-en-11-oyl)pyrrolidine-2-carboxamido)-4-methylpentanoate (**6g**)

The synthesis of unlabelled **6g** was performed as published elsewhere [20].

Synthesis of **ERW1041E** was performed according to published procedures (scheme 3) [9]. Analytical characterizations were in accordance with reported values [9, 23].

5.2.7.3. *(S)*-(3-bromo-4,5-dihydroisoxazol-5-yl)methanamine (**2**)

A solution of 50% glyoxylic acid (15.0 mL, 135 mmol) and hydroxylamine hydrochloride (9.40 g, 135 mmol) in H₂O (50 mL) was stirred for 2 h at rt. Sodium bicarbonate was added (22.7 g, 270 mmol) and the resulting solution was cooled on ice. Bromine was added dropwise (9.00 mL, 176 mmol) and the resulting solution was stirred overnight at rt. The mixture was extracted with DCM (3 times 100 mL). The combined organic fractions were dried on Na₂SO₄, filtered and carefully concentrated *in vacuo* to afford dibromoformaldoxime **1** as a white solid (14.1 g, 52%), which was

immediately used as such in the subsequent reaction. To a solution of allylamine hydrochloride (7.0 g, 75 mmol) in H₂O (100 mL) was added dibromoformaldoxime **1** (10 g, 49 mmol). To this solution was added dropwise a solution of KHCO₃ (6.0 g, 60 mmol) in H₂O (50 mL) over a three h period while stirring vigorously at rt. The resulting solution was stirred for another 3 h prior to dilution with saturated NaHCO₃ (100 mL). After extraction with DCM (3 times 100 mL), the combined organic fractions were dried on Na₂SO₄ and concentrated *in vacuo*. Flash column chromatography (DCM/MeOH, 9:1 (v/v)) afforded racemic (3-bromo-4,5-dihydroisoxazol-5-yl)methanamine as a yellow oil (5.1 g, 58%). Enantiomeric enrichment was performed as follows: to a solution of racemic (3-bromo-4,5-dihydroisoxazol-5-yl)methanamine (2.3 g, 12.9 mmol) and L-mandelic acid (1.0 g, 6.4 mmol) in hot MeOH was added dropwise hot isopropanol. The solution was allowed to cool to rt and left for 16 h. The solids were filtered off and recrystallization was performed out of a hot MeOH/isopropanol mixture until white crystalline needles were formed. After filtration, the needles were dissolved in saturated NaHCO₃ and the solution was extracted with DCM (3 times 20 mL). After drying on Na₂SO₄, filtration and concentration *in vacuo*, product **2** was obtained as a colourless oil 1.0 g, 87%). ¹H NMR (500 MHz, CDCl₃): δ 4.74 (m, 1H), 3.25 (dd, 1H, *J* = 17.4, 10.7 Hz), 3.08 (dd, 1H, *J* = 17.0, 7.8 Hz), 3.01 (dd, 1H, *J* = 13.5, 3.8 Hz), 2.58 (dd, 1H, *J* = 13.5, 5.7 Hz); ¹³C NMR (125 MHz, CDCl₃): δ 137.52, 83.11, 44.99, 43.85; ESI-HRMS: Calculated for C₄H₇BrN₂O: 177.9742, found: 178.9811 [M + H]⁺.

5.2.7.4. Quinolin-3-ylmethyl 1H-imidazole-1-carboxylate (**4**)

A solution of quinolone-3-carbaldehyde (2.50 g, 15.9 mmol) in ethanol/THF (20 mL) was cooled to -80 °C prior to the addition of LiBH₄ (0.34 g, 16 mmol). After stirring for 2 h, the mixture was quenched with 1 M HCl (100 mL) and allowed to reach rt. The resulting solution was diluted with saturated NaHCO₃ (100 mL) and extracted ethyl acetate (EtOAc) (3 times 50 mL). The collected EtOAc fractions were dried on Na₂SO₄, filtered and concentrated *in vacuo* to obtain quinolyn-3-ylmethanol as yellow oil.

Quinolyn-3-ylmethanol (2.40 g, 15.1 mmol) was dissolved in MeCN (10 mL) and carbonyldiimidazole (4.90 g, 30.2 mmol) was added to this solution. After stirring for 2 h at rt, the white precipitate was filtered and carefully washed with ice-cold acetonitrile (10 mL) obtaining compound **4** as a white solid (2.98 g, 78%). ¹H NMR (250 MHz, CDCl₃): δ 9.01 (d, 1H, *J* = 2.2 Hz), 8.27 (d, 1H, *J* = 2.1 Hz), 8.17-8.13 (m, 2H), 7.88 (dd, 1H, *J* = 8.1, 1.2 Hz), 7.79 (m, 1H), 7.61 (m, 1H), 7.44 (m, 1H), 7.07 (dd, 1H, *J* = 1.8, 0.9 Hz), 5.62 (s, 2H); ¹³C NMR (125 MHz, CDCl₃): δ 150.72, 148.65, 148.41, 137.25, 136.89, 131.01, 130.63, 129.53, 128.14, 127.55, 127.53, 126.87, 117.24, 67.61.

5.2.7.5. 2-methyl 1-(quinolin-3-ylmethyl) pyrrolidine-1,2-dicarboxylate (**5**)

To a solution of proline methyl ester hydrochloride (1.3 g, 7.9 mmol) and DiPEA (1.4 mL, 7.9 mmol) in DCM/DMF (1:1 (v/v), 10 mL) was added compound **4** (2.0 g, 7.9 mmol) in DCM (5 mL) and the solution was stirred at rt for 16 h. After concentrating *in vacuo*, the residue was dissolved in EtOAc and purified by flash column chromatography (hexane/EtOAc 3:2) obtaining compound **5** as a colourless oil (1.50 g, 60%). ¹H NMR (250 MHz, CDCl₃, mixture of rotamers): δ 8.93 and 8.87 (2x d, 1H, *J* = 2.2 Hz), 8.11 (dt, 1H, *J* = 12.1, 1.4 Hz), 7.84-7.79 (m, 1H), 7.75-7.66 (m, 1H), 7.58-7.51 (m, 1H), 5.41-5.20 (m, 2H), 4.37 (dt, 1H, *J* = 8.9, 3.8 Hz), 3.73-3.45 (m, 5H), 2.27-1.85 (m, 5H); ¹³C NMR (500 MHz, CDCl₃, mixture of rotamers): δ 173.21, 173.05, 154.66, 154.04, 150.82, 150.61, 147.92, 147.88, 135.53, 135.26, 129.77, 129.74, 129.73, 129.52, 129.48, 129.35, 128.00, 127.96, 127.73, 127.00, 64.89, 64.78, 59.31, 58.92, 52.40, 52.32, 47.10, 46.57, 31.01, 29.96, 24.40, 23.57; ESI-HRMS: Calculated for C₁₇H₁₈N₂O₄: 314.1267, found: 315.1348; 337.1158 [M + H]⁺, [M + Na]⁺.

5.2.7.6. (S)-1-((quinolin-3-ylmethoxy)carbonyl)pyrrolidine-2-carboxylic acid (**6**)

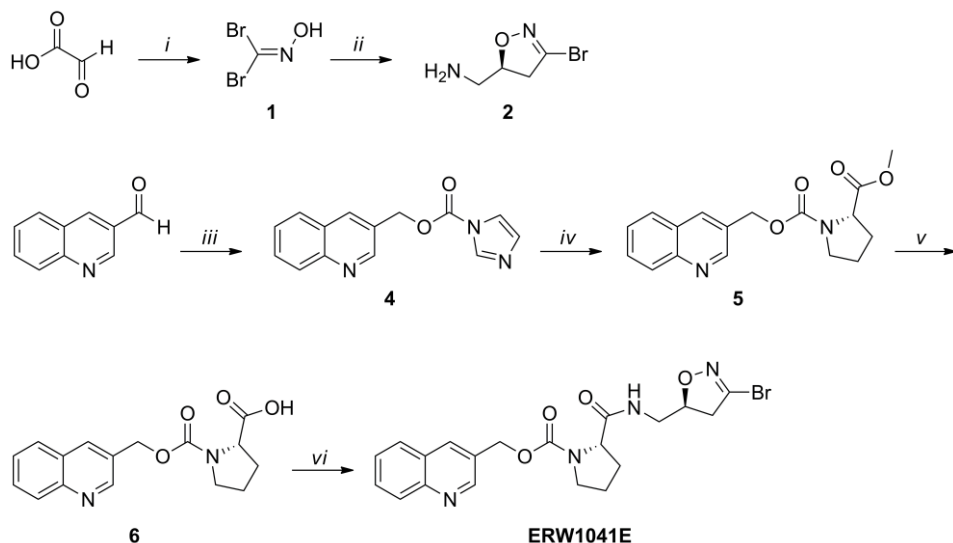
A solution of compound **5** (1.00 g, 3.18 mmol) in Tesser's base (dioxane/MeOH/4 M NaOH, 6:4:2 (v/v/v) 10 mL) was stirred for 2 h at rt prior to acidification to pH 4 with 1 M HCl. The solution was extracted with DCM (6 times 20 mL). The combined

organic fractions were dried on Na₂SO₄, filtered and concentrated *in vacuo*, obtaining compound **6** as a white solid (0.85 g, 89%). ¹H NMR (500 MHz, CDCl₃, mixture of rotamers): δ 11.32 (br s, 1H), 8.93 (s, 1H), 8.27 (s, 1H), 7.83-7.67 (m, 2H), 7.56-7.41 (m, 2H), 5.56 (d, 1H, *J* = 13 Hz), 5.09 (d, 1H, *J* = 12.6 Hz), 4.47-4.38 (m, 1H), 3.68-3.61 (m, 1H), 3.56-3.47 (m, 1H), 2.32-2.10 (m, 2H), 2.01-1.85 (m, 2H); ¹³C NMR (500 MHz, CDCl₃, mixture of rotamers): δ 175.58, 175.25, 154.97, 154.21, 149.16, 148.74, 144.34, 138.05, 137.38, 130.75, 130.70, 130.04, 128.07, 127.98, 127.89, 127.70, 127.61, 127.32, 125.98, 64.53, 64.19, 59.78, 59.45, 47.18, 46.72, 31.03, 29.88, 24.40, 23.71; ESI-HRMS: Calculated for C₁₆H₁₆N₂O₄: 300.1110, found: 301.1189; 323.1006 [M+H]⁺, [M+Na]⁺.

5.2.7.7. *(S)*-quinolin-3-ylmethyl 2-(((*S*)-3-bromo-4,5-dihydroisoxazol-5-yl)methyl)carbamoyl)pyrrolidine-1-carboxylate (**ERW1041E**)

A solution of carboxylic acid **6** (0.40 g, 1.3 mmol), amine **2** (0.24 g, 1.3 mmol), 1-ethyl-3-(3-dimethylaminopropyl)carbodiimide (EDC, 0.28 g, 1.5 mmol), hydroxybenzotriazole (HOBt, 0.20 mg, 1.3 mmol), *N*-methylmorpholine (0.15 mL, 1.3 mmol) in DMF (5 mL) was stirred for 2 h. The solution was concentrated *in vacuo* and the residue was purified by flash column chromatography (DCM/MeOH, 25:1 (*v/v*)), obtaining the product as colourless solid (0.59 g, 96%). ¹H NMR (500 MHz, CDCl₃, mixture of rotamers): δ 8.85 (m, 1H), 8.09 (m, 2H), 7.78 (m, 1H), 7.67 (m, 1H), 7.52 (m, 1H), 7.07-6.91 (m, 1H), 5.35-5.21 (m, 2H), 4.75-4.54 (m, 1H), 4.29 (m, 1H), 3.65-3.35 (m, 4H), 3.18-2.80 (m, 2H), 2.12-1.83 (m, 4H); ¹³C NMR (125 MHz, CDCl₃, mixture of rotamers): δ 173.19, 172.72, 155.32, 154.49, 150.63, 147.72, 138.00, 137.44, 135.56, 129.77, 129.22, 129.10, 127.91, 127.55, 126.94, 80.49, 80.21, 65.07, 64.89, 60.86, 60.63, 47.55, 47.05, 43.80, 43.62, 41.78, 41.23, 31.47, 29.59, 24.51, 23.59; ESI-HRMS: Calculated for C₂₀H₂₁BrN₄O₄: 460.0746, found: 461.0805, 483.0620 [M + H]⁺, [M + Na]⁺.

In vivo evaluation of two TG2 PET tracers in an orthotopic MDA-MB-231 tumour xenograft model



Scheme 3: Synthesis of **ERW1041E**. Reagents and conditions: *i*) hydroxylamine hydrochloride, H₂O, 2 h, room temperature (rt), then NaHCO₃, Br₂, 16 h, 0 °C to rt, 52%; *ii*) allylamine hydrochloride, KHCO₃, H₂O, 3 h, rt, 50%; *iii*) LiBH₄, ethanol/THF, 2 h, -80 °C, then CDI, MeCN, 2 h, rt, 78%; *iv*) proline methyl ester hydrochloride, DiPEA, DCM/DMF, 16h, rt, 60%; *v*) NaOH, dioxane/MeOH/H₂O, 2 h, rt, 89%; *vi*) amine **2**, EDC, HOBT, *N*-methylmorpholine, DMF, 2 h, rt, 96%.

5.2.8 PET imaging

Dynamic PET imaging was performed using dedicated small animal NanoPET/CT and NanoPET/MR scanners (Mediso Ltd., Hungary, Budapest) [24, 25] with identical PET components. Mice (n = 4 per group) were anaesthetized with 4% and 2% isoflurane in 1 L·min⁻¹ oxygen for induction and maintenance, respectively. Mice were positioned on the scanner bed and the respiratory rate was monitored for the duration of the scan, adjusting anaesthesia when required. A dynamic PET scan was acquired immediately after intravenous (i.v.) administration (tail vein) of 5 MBq [¹¹C]**3** or [¹⁸F]**6g**. For blocking experiments, mice were injected subcutaneously with **ERW1041E** (50 mg·kg⁻¹) dissolved in 20% dimethylsulfoxide in 0.9% saline, 30 min

prior to the tracer injection. An additional blocking experiment was performed by co-administration of compound **6g** (50 µg, 7.5 nmol) and [¹⁸F]**6g**, which corresponded with a specific activity of 0.7 GBq·µmol⁻¹. PET scans were acquired in list mode and rebinned into the following frame sequence: 4 × 5, 4 × 10, 2 × 30, 3 × 60, 2 × 300, 1 × 600, 1 × 900 and 1 × 1200 s. In addition, a static [¹⁸F]2-fluoro-2-deoxy-D-glucose ([¹⁸F]FDG) scan was acquired for 30 minutes immediately after [¹⁸F]FDG administration (10 MBq, tail vein). At least a 24 h time interval between [¹⁸F]FDG scans and [¹¹C]**3** or [¹⁸F]**6g** scans was maintained. Reconstruction was performed with a fully 3-dimensional (3D) reconstruction algorithm using 4 iterations and 6 subsets, resulting in an isotropic 0.4 mm voxel dimension. Images were analysed using the freely available AMIDE-software version 1.0.4 (retrieved from <https://sourceforge.net/projects/amide/files/amide/1.0.4>). Regions of interest (ROIs) were drawn around tumour tissue and leg muscle. Results are expressed as percentage injected dose per gram (%ID/g). Error bars indicate standard deviation. After PET scanning experiments, animals were sacrificed by cervical dislocation, tumours were isolated, and stored at -80 °C until further use.

5.2.9 Haematoxylin and eosin staining

MDA-MB-231 tumour sections (10 µm) were dried and fixed with acetone (100%) for 10 min and subsequently dried at rt. Sections were then rehydrated in Tris buffered saline (TBS, 2 times 5 min) and demiwater (5 min) and stained with Mayer's haematoxylin solution (3 min) followed by rinsing with tap water (5 min). The sections were stained with 1% eosin Y solution (10-30 s) followed by dehydrating by sequential dipping in ethanol (70, 90, 96, 100 and 100%) and xylene. Sections were then mounted with coverslips using Entellan. Microscopy images were obtained using a Leica DN5000B microscope (Leica Microsystems, IL, USA).

5.2.10 Immunohistochemical staining

Immunohistochemical staining of TG2 was performed as described previously with minor modifications [19]. Fresh frozen MDA-MB-231 tumour sections (10 µm) were dried and fixed with acetone (100%) for 10 min, dried at rt and subsequently rehydrated using TBS (3 times 5 min). Endogenous peroxidase activity was blocked with 0.3% H₂O₂ and 0.1% NaN₃ in TBS for 15 min and then washed with TBS (3 times 5 min). After blocking with 3% bovine serum albumin (BSA) in TBS with 0.5% TritonX-100 (TBS-T) for 20 min, incubation with polyclonal goat anti-guinea pig TG2 antibody (Upstate, Merck Millipore, Billerica, MA, USA) in TBS-T with 3% BSA was performed overnight at 4 °C (dilution 1:4000). A negative control experiment was performed by omitting the primary antibody (results not shown). Sections were then washed with TBS (3 times 5 min) prior to incubation with biotinylated donkey anti-goat secondary antibody (Jackson ImmunoResearch Laboratories Inc., West Grove, PA, USA, dilution 1:400) for 2 h at rt. Excess antibody was removed by washing with TBS (3 times 5 min) and sections were incubated for 1 h with horseradish peroxidase avidin-biotin complex. After sequential washing with TBS (2 times 5 min) and Tris-HCl (5 min), peroxidase mediated [1,1'-biphenyl]-3,3',4,4'-tetraamine (DAB) oxidation was used for visualizing TG2. Colouring was monitored *ad oculos*. After colouring was satisfactory, sections were washed sequentially with Tris-HCl (2 times 5 min) and water (5 min). Dehydration was carried out by sequential dipping in ethanol (70, 90, 96, 100 and 100%) and xylene, and sections were mounted with coverslips using Entellan. Microscopy images were obtained using a Leica DN5000B microscope (Leica Microsystems, IL, USA).

5.2.11 Histochemical staining

Histochemical staining of active TG2 was performed as described previously [19]. MDA-MB-231 tumour sections (10 µm) were pre-incubated in 100 mM Tris-HCl

buffer (pH 7.4), 5 mM CaCl₂, 1 mM dithiothreitol (DTT) rt (20 min). As negative control, the selective TG2 inhibitor **Z006** was added to this solution at a final concentration of 100 μM (results not shown). Next, sections were incubated in 100 mM Tris-HCl buffer (pH 7.4), 5 mM CaCl₂, 1 mM DTT and the TG2 amine donor substrate 5-(biotinamido)pentylamine (BAP, 0.05 mM) at 37 °C for 30 min. After a short wash with TBS and water, the sections were dried at rt. Then the sections were fixed with acetone for 10 min followed by washing with Tris buffered saline (TBS). Sections were blocked with 0.1% NaN₃ and 0.3% H₂O₂ in TBS for 15 min, washed with TBS (3 times 5 min) and incubated for 1 h with horseradish peroxidase avidin-biotin complex. After washing (2 times 5 min TBS, then 5 min Tris-HCl) peroxidase was developed by addition of DAB and colouring was monitored *ad oculos*. Nuclear staining using haematoxylin was performed. Sections were washed with Tris-HCl and water, dehydrated by sequential dipping in ethanol (70, 90, 96, 100 and 100%) and xylene, and mounted with coverslips using Entellan. Microscopy images were obtained using a Leica DN5000B microscope (Leica Microsystems, IL, USA).

5.2.12 Autoradiography

Autoradiography was performed essentially as described previously [20]. MDA-MB-231 tumour sections (10 μm) were washed three times with 50 mM Tris-HCl buffer (pH 7.4) for 5 min. Sections were dried under a gentle air flow before incubation for 30 min with [¹⁸F]**6g** (0.1 MBq·mL⁻¹) in 5 mM Tris-HCl, pH 7.4, 5 mM CaCl₂, 1 mM DTT. As a negative control inhibitor **3** was added to this incubation solution at 100 μM (results not shown). Washing was performed using 5 mM Tris-HCl (3 times) followed by dipping in ice cold water. After drying in an air stream, tumour sections were exposed to a phosphorimaging screen (GE Healthcare, Buckinghamshire, UK) for 15 min and developed on a Typhoon FLA 7000 phosphor imager (GE Healthcare, Buckinghamshire, UK). Visualization of binding was performed using ImageQuantTL v8.1.0.0 (GE Healthcare, Buckinghamshire, UK).

5.2.13 Statistical analysis

Where relevant, statistical analysis was performed using either a one-tailed paired Student's *t*-test or a two-tailed paired Student's *t*-test with a confidence interval of 95%.

5.3 Results

5.3.1 mRNA expression of various human transglutaminases in MDA-MB-231 cells and tumour xenograft tissue

The expression of various tumour related transglutaminases was determined by means of qPCR on both *in vitro* cultured MDA-MB-231 tumour cells and *ex vivo* MDA-MB-231 tumour material obtained after tumour inoculation in SCID mice. RNA expression levels of transglutaminase type 1-3, 5 and blood coagulation factor XIII (TG1, TG2, TG3, TG5 and FXIII) were quantitatively determined relative to GAPDH RNA expression (figure 3).

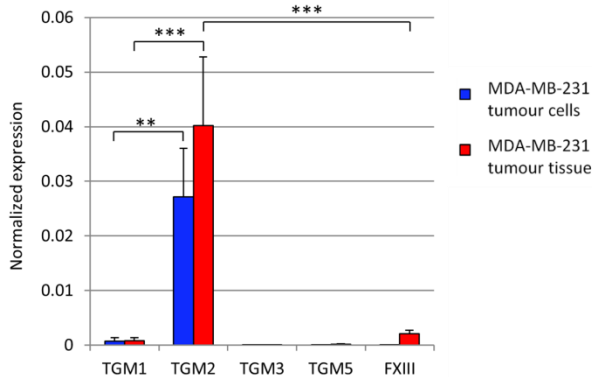


Figure 3: Transglutaminase mRNA expression in MDA-MB-231 tumour cells and in MDA-MB-231 tumour tissue. Results are expressed as relative values to GAPDH mRNA expression \pm standard deviation ($n = 4$; ** $p < 0.005$; *** $p < 0.0005$).

In MDA-MB-231 tumour cells as well as in tumour tissue, TG2 mRNA was most abundant. Low levels of TG1 mRNA were observed in both cells and tissue, whereas TG3 and TG5 mRNA were absent. FXIII mRNA was absent in cultured MDA-MB-231 tumour cells, whereas in tumour tissue low levels, relative to TG2 mRNA, were found.

5.3.2 Metabolite analysis of [¹¹C]**3** and [¹⁸F]**6g** in SCID mice

In SCID mice, compound [¹¹C]**3** demonstrated moderate metabolism, with 24% intact tracer after 45 min (table 2). Mainly polar metabolites were formed. [¹⁸F]**6g** was fully metabolized to a single metabolite after 45 min. The metabolite was identified by LC-MS/MS analysis as the demethylated parent **M1** (figure 4).

Table 2: Plasma metabolite profile of [¹¹C]**3** and [¹⁸F]**6g** following i.v. administration in healthy SCID mice and previously obtained results following i.v. administration in healthy Wistar rats [19, 20].

	[¹¹ C] 3		[¹⁸ F] 6g	
	Mouse	Rat	Mouse	Rat
15 min				
Intact tracer (%)	56 ± 14	65 ± 7	20 ± 1	1 ± 1
Non-polar metabolites (%)	24 ± 15	13 ± 4	76 ± 3	98 ± 1
Polar metabolites (%)	20 ± 5	21 ± 3	1 ± 0.2	2 ± 0
45 min				
Intact tracer (%)	24 ± 1	29 ± 11	3 ± 2	0 ± 0*
Non-polar metabolites (%)	28 ± 8	6 ± 3	95 ± 2	92 ± 3*
Polar metabolites (%)	47 ± 7	65 ± 12	2 ± 1	8 ± 3*

Following i.v. administration in healthy animals, anesthetized using isoflurane, blood plasma was obtained at 15 and 45 minutes. Blood plasma was separated into a polar and non-polar fraction using a SPE method. Non polar fractions were analysed on HPLC. Results are expressed as average percentage of total blood plasma activity ± standard deviation (n = at least 3 per data point). *Animals were sacrificed at 60 min post injection.

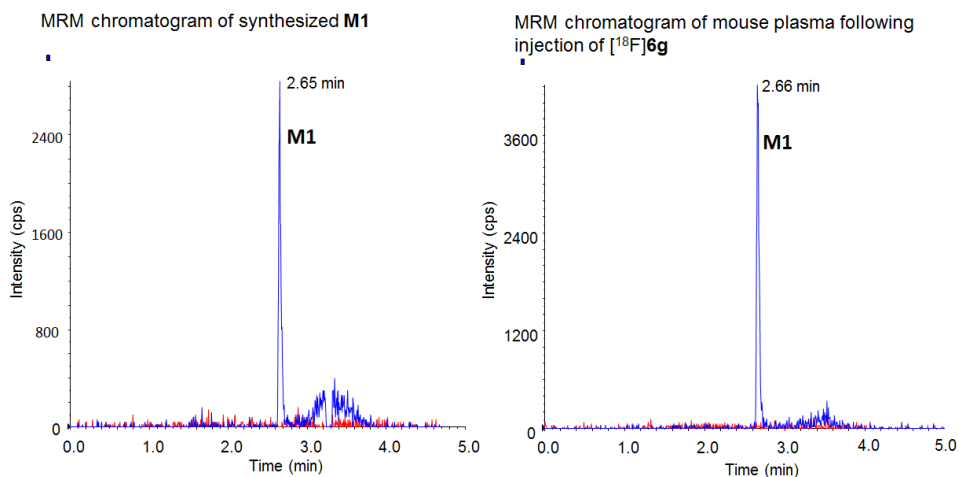


Figure 4: LC-MS/MS chromatograms of **M1** and following carrier added administration of [¹⁸F]**6g** to SCID mice. MRM mass transitions m/z 696.2-418.0 (Corresponding to **6g**, red line) and m/z 682.2-626.3 (Corresponding to **M1**, blue line). Left chromatogram: LC-MS/MS analysis of synthesized **M1**. Right chromatogram: LC-MS/MS analysis of mouse plasma after administration of [¹⁸F]**6g**. LC-MS/MS analysis indicated full conversion of **6g** to **M1**.

5.3.3 PET scanning

Representative images (0-30 min for [¹⁸F]FDG scans and last time-frame, 40-60 min, for [¹¹C]**3** and [¹⁸F]**6g**) and time-activity curves (TAC) of 60 min scans using [¹¹C]**3** and [¹⁸F]**6g** under both baseline and blocking conditions are depicted in figure 5A and 5B, respectively. The [¹⁸F]FDG scans revealed rather low uptake in the centres of the tumours, indicating mainly that the rims of the tumours were viable. Under baseline conditions, uptake of [¹¹C]**3** in the tumour at baseline conditions showed a peak at 5-10 min after injection (figure 5A). Washout, however, was fast and activity concentrations were comparable to those in background tissue (*i.e.* muscle, right femur). Furthermore, blocking of TG2 by pretreatment with **ERW1041E** did not result in lower tumour activity levels, but rather resulted in a counterintuitive significant increase in tumour activity, as well as in increased muscle activity concentration.

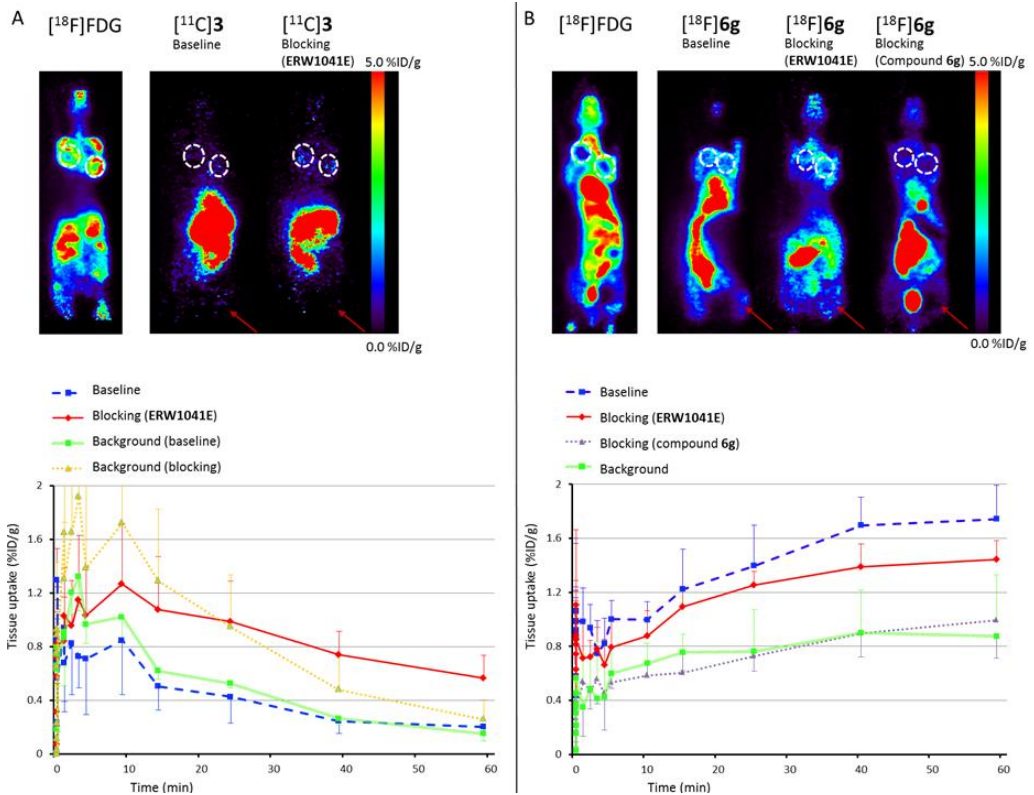


Figure 5: PET images and TACs of $[^{11}\text{C}]\mathbf{3}$ or $[^{18}\text{F}]\mathbf{6g}$ in MDA-MB-231 tumour bearing SCID mice ($n = 4$). Tumours are indicated with white dotted ellipses, background tissue (muscle) is indicated with a red arrow. A) Representative PET images of $[^{18}\text{F}]\text{FDG}$ scan and the last time-frame (40–60 min) after administration of $[^{11}\text{C}]\mathbf{3}$ under baseline and blocking conditions, and TACs of tumour under baseline (blue line) and blocking (red line) conditions and of background tissue under baseline (green line) and blocking (yellow line) conditions. B) Representative PET images of $[^{18}\text{F}]\text{FDG}$ scan and the last time-frame (40–60 min) under baseline conditions, and after blocking (ERW1041E) and self-blocking with $\mathbf{6g}$ after administration of $[^{18}\text{F}]\mathbf{6g}$, together with TACs of tumour under baseline (blue line) and blocking conditions (red and purple line), and of background tissue under baseline (green line) conditions.

PET scanning using compound [^{18}F]**6g** showed a time-dependent accumulation in tumour tissue up to 1.7 %ID/g at the 40-60 min time-frame, suggesting irreversible tumour targeting. Background values (muscle, right femur) reached 0.8 %ID/g at this time-point, which is significantly lower ($p = 0.0004$) and did not display an increase in tissue activity over the scanning period (figure 5B). Pretreatment of the animals with the TG2 inhibitor **ERW1041E** resulted in a decrease in activity accumulation in the tumour tissue to 1.4 %ID/g, although this difference was not statistically significant ($p = 0.06$). A drastic and significant decrease in tumour activity concentration, however, was observed when unlabelled **6g** was co-administered, to approximately 1.0 %ID/g ($p = 0.007$).

5.3.4 TG2 expression in MDA-MB-231 tumour tissue - immunohistochemistry and autoradiography on tumour tissue

Following sacrifice of the animals, tumour sections were evaluated histochemically for TG2 expression and TG2 activity (representative sections of tumour tissues of three separate animals are shown in figure 6).

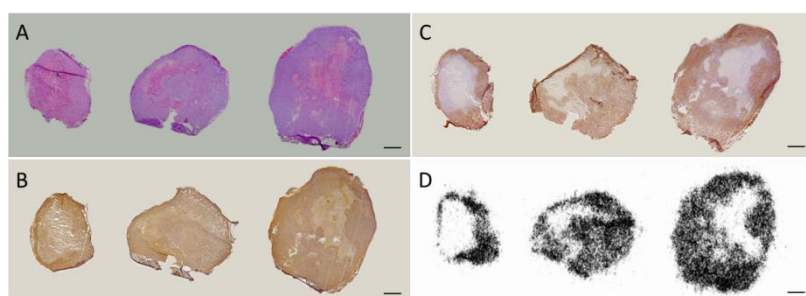


Figure 6: Immunohistochemistry and autoradiography on representative MDA-MB-231 tumour sections (adjacent) obtained from three representative tumours used in this study. A) Haematoxylin/eosin staining; B) immunohistochemical detection of TG2; C) TG2 mediated incorporation of BAP; D) autoradiography using [^{18}F]**6g**. Scale bars: 1 mm.

In all tumours, haematoxylin/eosin staining (figure 6A) demonstrated areas with low nuclei concentrations in the core of the tumour, hinting at central necrosis. Immunohistochemical staining for TG2 expression (figure 6B) resulted in a distribution pattern highly resembling the haematoxylin/eosin staining, showing that TG2 is predominantly expressed in the viable part of the tumours. Transglutaminase mediated BAP incorporation (figure 6C) and *in vitro* autoradiography employing [¹⁸F]**6g** (figure 6D), both means of measuring the open (active) conformation of transglutaminase, demonstrated a similar distribution pattern as observed with the anti-TG2 antibody and the haematoxylin/eosin staining, *i.e.* incorporation of the substrate and inhibitor in the viable areas of tumour tissue.

5.4 Discussion

Transglutaminase mRNA expression in both MDA-MB-231 tumour cells and xenograft tissue essentially was limited to TG2 mRNA, and exceeded other transglutaminases by at least a factor ten. The detection of FXIII mRNA in tumour tissue, which is most likely derived from the blood component of the tumour tissue, does not hamper the use of both [¹¹C]**3** and [¹⁸F]**6g** TG2 PET tracers, as both compounds show no affinity for activated FXIII [19, 20]. Consequently, these findings imply that the MDA-MB-231 xenograft model is suitable for TG2 PET tracer evaluation.

Previously, metabolic stability of [¹¹C]**3** as well as [¹⁸F]**6g** was determined *ex vivo* in blood plasma of healthy Wistar rats. This study, however, was performed in a xenograft model in SCID mice and, therefore, the metabolic stability of both radiotracers was determined again in SCID mice and results were compared with previously obtained rat data [19, 20]. Metabolism of both [¹¹C]**3** and [¹⁸F]**6g** in SCID mice highly resembled metabolism of these compounds in Wistar rats. Conversion of [¹⁸F]**6g** to the demethylated analogue **M1**, still a potent TG2 inhibitor, followed the same pattern in both species, although in mice the conversion was less rapid. This

difference is likely a result of species dependent esterase activity [26] and comparable differences between methylester hydrolysis in mice and rats have been reported elsewhere [27]. Importantly, the peptidic backbone and the diazoketone functionality in [¹⁸F]**6g**, responsible for selective and irreversible binding, respectively, appear metabolically stable.

To prevent the development of slow-growing and highly necrotic tumours, an orthotopic mouse model was used, in which tumour cells were inoculated in the 2nd thoracic mammary fat pad [21]. At this position minimal interference with surrounding organs such as liver and heart is expected, thus facilitating definition of ROIs and PET data analysis. The use of the structurally unrelated TG2 inhibitor **ERW1041E** served as a means of determining selectivity of binding of TG2 radiotracers in tumour tissue. **ERW1041E** was administered at 50 mg·kg⁻¹, as it has been shown that this dose results in inhibition of TG2 activity to background levels in a mouse model of pulmonary hypertension [9]. In addition, the maximum TG2 inhibitory effect was observed 30 min after **ERW1041E** administration [9].

Compound [¹¹C]**3** showed poor tumour uptake and relatively fast washout from the tumour, which was unexpected for an irreversibly binding radiotracer. Therefore, it is believed that the signal is indicative of perfusion rather than TG2 targeting. The fact that both tumour and muscle activity concentrations increased as a result of **ERW1041E** pretreatment suggests to us a decreased clearance of [¹¹C]**3** or its derived radioactive metabolites from blood, although no further experiments were performed to support this claim. Despite the promising results that were previously obtained by *in vitro* autoradiography, where high specific and selective binding of [¹¹C]**3** to MDA-MD-231 tumour sections was observed [19], [¹¹C]**3** is not effective as a TG2 PET tracer *in vivo*. It is unlikely that this apparent ineffectiveness is a result of *in vivo* metabolism of [¹¹C]**3** over the time-course of these experiments, as metabolism is moderate. Potentially, large differences between *in vitro* TG2 inhibitory potency

and inhibition in actual biological systems could explain the inability of this compound to image active TG2 *in vivo*. Different classes of acryl amide based TG2 inhibitors, although highly potent against isolated TG2, have shown a reduction in inhibitory potency in cell or cell lysate assays [28, 29]. The inhibitory potency of compound **3** in similar cell or cell lysate assays is unknown as such experiments have not been described [30].

In contrast to [¹¹C]**3**, [¹⁸F]**6g** displayed higher tumour uptake, which increased over time, indicating irreversible binding of [¹⁸F]**6g** to the tumour tissue. Uptake decreased after pretreating animals with **ERW1041E**, although the difference was not statistically significant ($p = 0.06$). This seemingly partial inhibition of TG2 might be due to the limited TG2 inhibitory potency of **ERW1041E** (K_i : 11 μ M [23]) compared with compound **6g**, although previously it has been shown that this compound was able to at least partially inhibit intestinal TG2 in a mouse model [8] and also in a mouse model of pulmonary hypertension to baseline levels [9]. Alternatively, the chosen time-point for pretreatment with **ERW1041E** (set at 30 min prior to tracer administration) might not be optimal for full TG2 inhibition, although at this similar time-point a reduction of TG2 activity by a factor of four in a pulmonary hypertension model was observed [9]. The blocking effect when co-administering unlabelled **6g** and [¹⁸F]**6g** ($p = 0.007$), implies that [¹⁸F]**6g** is useful for imaging of local TG2 activity *in vivo* by indicating specific binding of [¹⁸F]**6g**. However, to establish the selectivity of this uptake, more studies are required.

Analysis of tumour sections showed that TG2 was expressed mainly in the more viable rim of the tumours and less in the necrotic core of the tumours. This decreased tumour viability in the core of the tumours is in close accordance with [¹⁸F]FDG findings, which generally displayed higher uptake in the outer tumour areas. Because %ID/g was determined by drawing an area over the full tumour volume, areas inside the tumour that contain no tissue transglutaminase potentially underestimate the

actual potential of [¹⁸F]**6g** towards TG2 targeting. As PET images using [¹⁸F]**6g** depicted higher activity concentrations in the outer area of the tumour, for future research it might prove beneficial to perform such an imaging study at an earlier time-point in tumour development, potentially limiting tumour necrosis and thus increasing signal to noise ratios.

Although previously relatively high tissue transglutaminase expression levels in MDA-MB-231 tumour cell lysates were observed [10], and both TG2 expression and activity were further confirmed in xenografted MDA-MB-231 tumour tissue by means of immunohistochemistry and *in vitro* autoradiography [19, 20], it is unknown to what extent TG2 shows transamidation activity in a biological setting such as the present MDA-MB-231 tumour model. Obviously, only in the open TG2 conformation, active site directed PET tracers can be successfully applied for TG2 imaging [5, 18]. Therefore, it is expected that primarily extracellular TG2, which is more likely to be in an open conformation due to high extracellular calcium concentrations, will be accessible for such tracers [18]. Previous *in vitro* studies have demonstrated that TG2 is highly expressed on the plasma membrane of MDA-MB-231 tumour cells [31]. Furthermore, pharmacological inhibition of TG2 on MDA-MB-231 cells using cell-impermeable small molecule inhibitors or antibodies resulted in decreased cell migration [31, 32] and decreased invasiveness [33], which both are hallmarks of cancer [34]. Based on these findings it is expected that the accumulation of activity in the tumour using [¹⁸F]**6g** is due to targeting of extracellular TG2. Evidence suggests that extracellular TG2 plays a role in tumour progression by means of its transamidation activity and therefore the MDA-MB-231 tumour model appears suitable for evaluation of TG2 PET tracers *in vivo*, which is supported by the imaging results using [¹⁸F]**6g**. Together, the *in vivo* targeting of TG2 PET tracers is evaluated for the first time and the results suggest that [¹⁸F]**6g** could be used in future research, for example for evaluation of target engagement of other TG2 inhibitors.

5.5 Conclusion

TG2 PET tracers [^{11}C]**3** and [^{18}F]**6g** were evaluated in an MB-MDA-231 breast cancer mouse model. Whereas the TG2 targeting potential of [^{11}C]**3** in this model seemed inadequate, [^{18}F]**6g** showed signs of TG2 targeting, as tumour activity concentrations were steadily increasing over time and could be blocked with TG2 inhibitors.

5.6 References

- [1] Greenberg CS, Birckbichler PJ, Rice RH. Transglutaminases: multifunctional cross-linking enzymes that stabilize tissues. *FASEB J* **1991**; 5: 3071-3077.
- [2] Gundemir S, Colak G, Tucholski J, et al. Transglutaminase 2: A molecular Swiss army knife. *Biochim Biophys Acta Mol Cell Res* **2012**; 1823: 406-419.
- [3] Fesus L, Szondy Z. Transglutaminase 2 in the balance of cell death and survival. *FEBS Lett* **2005**; 579: 3297-3302.
- [4] Liu S, Cerione RA, Clardy J. Structural basis for the guanine nucleotide-binding activity of tissue transglutaminase and its regulation of transamidation activity. *PNAS* **2002**; 99: 2743-2747.
- [5] Pinkas DM, Strop P, Brunger AT, et al. Transglutaminase 2 undergoes a large conformational change upon activation. *PLoS Biology* **2007**; 5: 2788-2796.
- [6] Stammaes J, Pinkas DM, Fleckenstein B, et al. Redox regulation of transglutaminase 2 activity. *J Biol Chem* **2010**; 285: 25402-25409.
- [7] Akimov SS, Krylov D, Fleischman LF, et al. Tissue transglutaminase is an integrin-binding adhesion coreceptor for fibronectin. *J Cell Biol* **2000**; 148: 825-838.
- [8] Dafik L, Albertelli M, Stammaes J, et al. Activation and inhibition of transglutaminase 2 in mice. *PLoS ONE* **2012**; 7: e30642.
- [9] DiRaimondo TR, Klöck C, Warburton R, et al. Elevated transglutaminase 2 activity is associated with hypoxia-induced experimental pulmonary hypertension in mice. *ACS Chem Biol* **2013**; 9: 266-275.
- [10] Mehta K, Fok J, Miller FR, et al. Prognostic significance of tissue transglutaminase in drug resistant and metastatic breast cancer. *Clin Cancer Res* **2004**; 10: 8068-8076.
- [11] Brown KD. Transglutaminase 2 and NF- κ B: an odd couple that shapes breast cancer phenotype. *Breast Cancer Res Treat* **2013**; 137: 329-336.
- [12] Klöck C, DiRaimondo TR, Khosla C. Role of transglutaminase 2 in celiac disease pathogenesis. *Semin Immunopathol* **2012**; 34: 513-522.

- [13] Olsen KC, Sapinoro RE, Kottmann RM, et al. Transglutaminase 2 and its role in pulmonary fibrosis. *Am J Respir Crit Care Med* **2011**; 184: 699-707.
- [14] Johnson TS, Griffin M, Thomas GL et al. The role of transglutaminase in the rat subtotal nephrectomy model of renal fibrosis. *J Clin Invest* **1997**; 99: 2950-2960.
- [15] Wilhelmus MMM, van Dam A, Drukarch B. Tissue transglutaminase: A novel pharmacological target in preventing toxic protein aggregation in neurodegenerative diseases. *Eur J Pharmacol* **2008**; 585: 464-472.
- [16] De Laurenzi V, Melino G. Gene Disruption of Tissue Transglutaminase. *Mol Cell Biol* **2001**; 21: 148-155.
- [17] Keillor JW, Apperley KYP, Akbar A. Inhibitors of tissue transglutaminase. *Trends Pharmacol Sci* **2015**; 36: 32-40.
- [18] Van der Wildt B, Lammertsma AA, Drukarch B, et al. Strategies towards in vivo imaging of active transglutaminase type 2 using positron emission tomography. *Amino Acids* **2016**; doi: 10.1007/s00726-016-2288-y.
- [19] Van der Wildt B, Wilhelmus MMM, Bijkerk J, et al. Development of carbon-11 labeled acryl amides for selective PET imaging of active tissue transglutaminase. *Nucl Med Biol*. **2016**; 43: 232-242.
- [20] Van der Wildt B, Wilhelmus MMM, Kooijman EJM, et al. Development of fluorine-18 labelled peptidic PET tracers for imaging active tissue transglutaminase. *Nucl Med Biol* **2017**; 44: 90-104.
- [21] Price JE, Polyzos A, Zhang RD et al. Tumorigenicity and metastasis of human breast carcinoma cell lines in nude mice. *Cancer Res* **1990**; 50: 717-721.
- [22] Ruijter JM, Ramakers C, Hoogaars WM, et al. Amplification efficiency: linking baseline and bias in the analysis of quantitative PCR data. *Nucleic Acids Res* **2009**; 37: e45.
- [23] Watts RE, Siegel M, Khosla C. Structure-activity relationship analysis of the selective inhibition of transglutaminase 2 by dihydroisoxazoles. *J Med Chem* **2006**; 49: 7493-7501.

- [24] Szanda I, Mackewn J, Patay G, et al. National electrical manufacturers association NU-4 performance evaluation of the PET component of the NanoPET/CT preclinical PET/CT scanner. *J Nucl Med* **2011**; 52: 1741-1747.
- [25] Nagy K, Tóth M, Major P, et al. Performance evaluation of the small-animal nanoScan PET/MRI System. *J Nucl Med* **2013**; 54: 1825-1832.
- [26] Bahar FG, Ohura K, Ogihara T. Species difference of esterase expression and hydrolase activity in plasma. *J Pharmacol Sci* **2012**; 101: 3979-3988.
- [27] Slobbe P, Poot AJ, Haumann R, et al. Two anti-angiogenic TKI-PET tracers, [¹¹C]axitinib and [¹¹C]nintedanib: Radiosynthesis, in vivo metabolism and initial biodistribution studies in rodents. *Nucl Med Biol* **2016**; 43: 612-624.
- [28] Prime ME, Andersen OA, Barker JJ, et al. Discovery and structure–activity relationship of potent and selective covalent inhibitors of transglutaminase 2 for Huntington’s disease. *J Med Chem* **2012**; 55: 1021-1046.
- [29] Badarau E, Wang Z, Rathbone DL et al. Development of potent and selective tissue transglutaminase inhibitors: their effect on TG2 function and application in pathological conditions. *Chem Biol* **2015**; 22: 1347-1361.
- [30] Wityak J, Prime ME, Brookfield FA, et al. SAR development of lysine-based irreversible inhibitors of transglutaminase 2 for Huntington's disease. *ACS Med Chem Lett* **2012**; 3: 1024-1028.
- [31] Antonyak MA, Li B, Regan AD, et al. Tissue transglutaminase is an essential participant in the epidermal growth factor-stimulated signaling pathway leading to cancer cell migration and invasion. *J Biol Chem* **2009**; 284: 17914-17925.
- [32] Wang Z, Griffin M. The role of TG2 in regulating S100A4-mediated mammary tumour cell migration. *PLoS ONE* **2013**; 8: e57017.
- [33] Mangala LS, Fok JY, Zorrilla-Calanca IR, et al. Tissue transglutaminase expression promotes cell attachment, invasion and survival in breast cancer cells. *Oncogene* **2007**; 26: 2459-2470.
- [34] Hanahan D, Weinberg RA. The Hallmarks of Cancer. *Cell* **2000**; 100: 57-70.

